WINDAGE POWER LOSS IN SPUR GEAR SETS

FAKHER CHAARI, MANEL BEN ROMDHANE, WALID BACCAR,
TAHER FAKHFAKH, MOHAMED HADDAR
Mechanics Modelling and Production research Unit
National School of Engineers of Sfax
BP 1173 - 3038 – Sfax – TUNISIA
Fakher.chaari@gmail.com ; benromdhanemanel@yahoo.fr ; walid_baccar@yahoo.fr ;
Tahar.Fakhfakh@enis.rnu.tn ; mohamed.haddar@enis.rnu.tn

Abstract: - The windage power loss in gear transmission systems at high speeds can be significant and must be taken into account at the design stage in order to optimize the geometrical shape of the gear's bodies to improve the mechanical efficiency. The main objective of this work is, first, to propose a design of a two-dimensional geometry of the spur gear using the commercial Computational Fluid Dynamics (CFD) Fluent 6.3.26 which enable us to detect the pressure and viscous moments due to the aerodynamic drag of the teeth in the air-lubricant mixture. In addition, a parametric study concerning the influence of the geometrical shape of teeth and the lubricant on the evolution of the windage power losses on the gear teeth is carried out.

Key-Words: - windage power loss, spur gear, CFD, lubrication, addendum modification.

1 Background

1.1 Introduction

Gear transmission sets are systems used for transmitting power, i.e. starting from a power provided by the external medium (generally an electric motor), gear can transmit power to a receiver. This power transmission cannot be achieved without losses or dissipation of heat within the transmission. Among these losses we can distinguish those by friction resulting from contact between teeth in mesh which constitute a major source of dissipation at low rotational speeds (Chaari et al., 2010). The other important loss is that caused by churning which represents the power lost because of the compression of the air-lubricant mixture around teeth roots during meshing. The third power loss is that induced by windage (WPL), which corresponds to the power lost because of the aerodynamic trail of the teeth in the air-lubricant mixture. It is assumed that the WPL control the total efficiency of the system in the case of high operating speeds. So, these power losses must be taken into account by designers in order to optimize the geometrical shape of the gears with the principal objective which is the reduction of the energy losses and the improvement of the mechanical efficiency.

In this paper we will be interested in the windage power component of the total power loss.

1.2 Previous work

If we focus on windage power losses, few research works were developed. Townsend and Dudley (Townsend et al., 1992) proposed two equations according to the teeth geometry (spur gear or helical gear), to calculate the WPL of a gear set. In their approaches, the power loss is proportional to the cube number of rotational speed and the quintuplicate of the gear diameter. Indeed, for the spur gears, the power losses depend on parameters associated with the operating conditions and the geometry of the gears, but for the helical gears, the power loss breaks up into two parts, one related to teeth and the other with the sides of gears.

Anderson (Neil et al., 1980) established a formula for pinion-gear system, rotating in a gearbox containing a mixture air-oil.

In addition, Dawson (Dawson, 1984) (Dawson, 1988) led a series of experiments on large diameters gears for a maximum number of rotational speeds not exceeding 750 rpm. He proposed two equations in which one took into account the air conditions surrounding the teeth (the kinematic viscosity of the

lubricant). Moreover, according to Dawson, the loss generated by a gearbox corresponds almost to the sum of the losses of each gear taken individually (error lower than 3%).
Using the same methodology of Dawson, Diab (Diab et al.,2004) developed a test rig specifically to measure the WPL. He showed that this kind of loss is over-estimated by using the formulas of Dawson. In addition, Diab developed two theoretical approaches: the first one is based on a dimensional analysis of the various significant factors allowing the establishment of an expression of the total drag moment as function of the most influencing parameters of the system. The other one is based on the circulation of the fluid on the periphery and the sides of the wheels. These theoretical approaches were in agreement with his experimental work. However, the expression of the power losses given by Diab does not take into account of the state of mesh, and then the component resulting from the churning of the air or the mixture air-oil in the tooth root. This parameter was treated by Seetharaman (Seetharaman, 2009) in his computation of the WPL for a gear pair (considering lubrication with injection).
In another way, by using a commercial computational fluid dynamics code (CFD), Al-Shibl (Al-Shibl, 2007) developed a two-dimensional model of a spur gear which enabled him to compute the WPL on the periphery for a single spur gear rotating in the air, the losses on the sides are recovered by using the formula of Townsend (Al-Shibl, 2007). Eastwick and Johnson (Eastwick, 2008) supplied an extensive review of studies on gear windage to conclude that the general solution for reducing power loss due to windage has not yet been well-established.

2 Methodology

In this paper, we are interested in the quantifications of the WPL for spur gears, by using the commercial computational fluid dynamics software "Fluent". Such numerical codes became very attractive tools for the prediction of the fluid flow in many fields of engineering since they can be considered as a true ″numerical experiment″. A parametric study will be made in order to put in evidence their influence on the WPL.

2.1 Numerical method

2.1.1 Governing equations

The fundamental equations of the fluid mechanics for instance, the conservation equations of mass and momentum, can be written as follows (Fluent, 2006)

$$\frac{\partial}{\partial x_i}\rho U_i = 0 \tag{1}$$

$$\underbrace{\frac{\partial}{\partial x_i}(\rho U_i U_j)}_{(A)} = \underbrace{-\frac{\partial P}{\partial x_i}}_{(B)} + \underbrace{\frac{\partial \tau_{ij}}{\partial x_j}}_{(C)} + \underbrace{\rho g_j}_{(D)} \tag{2}$$

In equation (2), (A) is the convective term, (B) represent the pressure effect, (C) the diffusion term and (D) the effect of gravity (negligible term in our case).
Simulations were based on the RSM (Reynolds Stress Model) mathematical model of turbulence. The exact transport equations for the transport of the Reynolds stresses $\rho\overline{u_i' u_j'}$ may be written as follows (Fluent, 2006):

$$\underbrace{\frac{\partial}{\partial t}(\rho\overline{u_i' u_j'})}_{(1)} + \underbrace{\frac{\partial}{\partial x_k}(\rho U_k \overline{u_i' u_j'})}_{(2)} =$$

$$\underbrace{-\frac{\partial}{\partial x_k}\left[\rho\overline{u_i' u_j' u_k'} + \overline{p(\delta_{kj}u_i' + \delta_{ik}u_j')}\right]}_{(3)} + \underbrace{\frac{\partial}{\partial x_k}\left[\mu\frac{\partial}{\partial x_k}(\overline{u_i' u_j'})\right]}_{(4)}$$

$$\underbrace{-\rho\left[\overline{u_i' u_k'}\frac{\partial u_j}{\partial x_k} + \overline{u_j' u_k'}\frac{\partial u_i}{\partial x_k}\right]}_{(5)} \underbrace{-\rho\beta(g_i\overline{u_j'\theta} + g_j\overline{u_i'\theta})}_{(6)}$$

$$\underbrace{+\overline{p\left(\frac{\partial u_i'}{\partial x_j} + \frac{\partial u_j'}{\partial x_i}\right)}}_{(7)} \underbrace{-2\mu\overline{\frac{\partial u_i'}{\partial x_k}\frac{\partial u_j'}{\partial x_k}}}_{(8)}$$

$$\underbrace{-2\rho\Omega_k(\overline{u_j' u_m'}\varepsilon_{ikm} + \overline{u_i' u_m'}\varepsilon_{jkm})}_{(9)} + \underbrace{S_{user}}_{(10)} \tag{3}$$

In equation 3, (1) is the local time derivation, (2) represent the convection term (C_{ij}), (3) the turbulent diffusion($D_{T,ij}$), (4) the molecular diffusion($D_{L,ij}$), (5) the stress production (P_{ij}), (6) is the buoyancy production (G_{ij}), (7) the pressure strain (ϕ_{ij}), (8) represent the term of dissipation (ε_{ij}), (9) the production by system rotation (F_{ij}) and (10) is the user-defined source term.
Of the various terms in these exact equations, C_{ij}, $D_{L,ij}$, P_{ij}, and F_{ij} do not require any modelling. However, $D_{T,ij}$, G_{ij}, ϕ_{ij}, and ε_{ij} need to be modelled to close the equations.

$D_{T,ij}$ can be modeled by the generalized gradient-diffusion model of Daly and Harlow (Daly et al., 1970):

$$D_{T,ij} = C_s \frac{\partial}{\partial x_k}\left(\rho k \frac{\overline{u_k' u_\ell'}}{\varepsilon}\frac{\partial \overline{u_i' u_j'}}{\partial x_\ell}\right) \quad (4)$$

However, this equation can result in numerical instabilities, so it has been simplified in Fluent to use a scalar turbulent diffusivity as follows (Lien, 1994):

$$D_{L,ij} = \frac{\partial}{\partial x_k}\left(\frac{\mu_t}{\sigma_k}\frac{\partial \overline{u_i' u_j'}}{\partial x_k}\right) \quad (5)$$

where μ_t is the turbulent viscosity, and σ_k=0.82.

By default in Fluent, The classical approach to model the pressure-strain term ϕ_{ij} is to consider the following decomposition (Fluent, 2006):

$$\phi_{ij} = \phi_{ij,1} + \phi_{ij,2} + \phi_{ij,\omega} \quad (6)$$

where $\phi_{ij,1}$ is the slow pressure-strain term, also known as the return-to-isotropy term, $\phi_{ij,2}$ is called the rapid pressure-strain term, and $\phi_{ij,\omega}$ is the wall-reflection term.

The slow pressure-strain term, $\phi_{ij,1}$, is modelled as

$$\phi_{ij,1} = -C_1 \rho \frac{\varepsilon}{k}\left[\overline{u_i' u_j'} - \frac{2}{3}\delta_{ij} k\right] \quad (7)$$

with $C_1 = 1.8$.

The rapid pressure-strain term, $\phi_{ij,2}$, is modelled as

$$\phi_{ij,2} = -C_2\left[(P_{ij} + F_{ij} + G_{ij} - C_{ij}) - \frac{2}{3}\delta_{ij}(P + G - C)\right] \quad (8)$$

where $C_2 = 0.60$, P_{ij}, F_{ij}, G_{ij}, and C_{ij} are defined as in Equation (3), $P = \frac{1}{2}P_{kk}$, $G = \frac{1}{2}G_{kk}$, and $C = \frac{1}{2}C_{kk}$.

The wall-reflection term, $\phi_{ij,\omega}$, is responsible for the redistribution of normal stresses near the wall. It tends to damp the normal stress perpendicular to the wall, while enhancing the stresses parallel to the wall. This term is modelled as :

$$\phi_{ij,\omega} = C_1''\frac{\varepsilon}{k}\left(\overline{u_k' u_m'} n_k n_m \delta_{ij} - \frac{3}{2}\overline{u_i' u_k'} n_j n_k - \frac{3}{2}\overline{u_j' u_k'} n_i n_k\right)\frac{k^{\frac{3}{2}}}{C_\ell \varepsilon d}$$
$$+ C_2''\left(\phi_{km,2} n_k n_m \delta_{ij} - \frac{3}{2}\phi_{ik,2} n_j n_k - \frac{3}{2}\phi_{jk,2} n_i n_k\right)\frac{k^{\frac{3}{2}}}{C_\ell \varepsilon d} \quad (9)$$

where C_1''=0.5, C_2''=0.3 , n_k is the x_k component of the unit normal to the wall, d is the normal distance to the wall, and $C_1 = \frac{C_\mu^{\frac{3}{4}}}{\kappa}$, where C_μ=0.09 and k=0.4187 is the von Kármán constant.

2.1.2 CFD code presentation

The CFD software Fluent is widely used in the aircraft and automobile industry. It offers an interactive interface which facilitates its use. Indeed, Fluent models by the finite volume method different kinds of flows in complex configurations. Moreover, Fluent simulates all the fluid flows, compressible or incompressible, involving complex physical phenomenon such as the turbulence, heat transfer, and chemical reactions. Like any CFD software, it is composed of three key elements: pre-processor, processor and the post-processor (figure1) (Fedala, 2007).

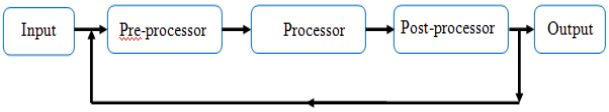

Fig.1 Graphical representation of CFD software

The pre-processor Gambit: It is used to build the geometry of the model and to subdivide it into small control volumes or cells, all of these elementary volumes constitutes the mesh. Also, it allows the definition of the boundary condition of the model (wall, periodicity, symmetry...), specify the type of the material (fluid and solid) and to create several kinds of mesh depending on the geometry. It generates msh files used by Fluent.

The processor Fluent 6.3.26: allows to define the numerical operating conditions (rotational speed, pressure, periodicity condition) in which the simulation is performed, as well as the specification of the boundary conditions. It makes possible to choose the iterative process, by offering several numerical schemes for the spatial and temporal discretization and for the pressure velocity coupling.

The discretized equations are solved and described as: convection – diffusion = sources – loss. For incompressible fluids, the computations are done in relative pressure. The finite volume method is used, this method has the advantage of being conservative, i.e. that all the outflow of a control volume enters in the neighbouring volumes. The computation steps are as follows:

- Integration of the continuous equations on each volume of control. Ostrogradski theorem is used to transform some volume integrals into surface integrals.
- Discretization in space and time (for non-permanent flows) of the equations: substitution of partial derivatives by approximations with finite difference method and then transformation of the system of equations into algebraic system.
- Resolution of the algebraic system by iterative process, using an algorithm to correct the pressure and the velocity components in order to ensure the conservation of mass. A graphical interface makes possible the control of the residual values according to the iteration count.

The post-processor: allows viewing geometry, mesh field, and results i.e. the static pressure cartographies, relative velocities and the temperature fields. The post processor allows plotting the results as profiles and streamlines.

2.2 Geometry of the system

In order to measure WPL of the gear, 4 spur gear having the characteristics given in table 1 are considered:

designation	Teeth number	Thickness of gear [mm]	Module [mm]	Pressure angle [°]	Addendum modification
Gear n°1	120	40	1	20	0
Gear n°2	25	40	8	20	0
Gear n°3	25	40	8	20	0.5
Gear n°4	25	40	1	20	0

Table1. Geometrical characteristics of the studied gears

There gears are rotating in a cylindrical gearbox containing a lubricant as presented in figure 2.

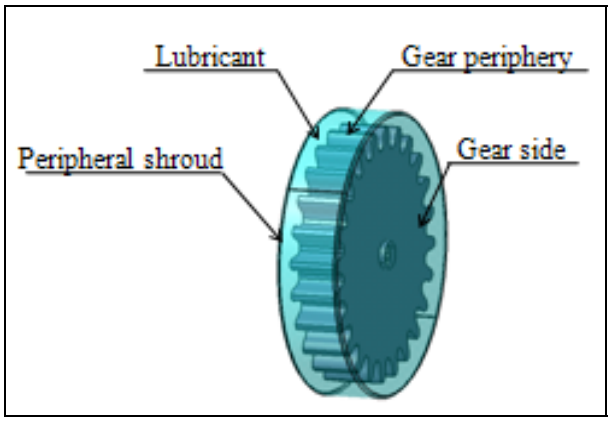

Fig.2 Scheme of the modelled gear

2.2.1 Meshing

A two dimensional model of the gear is developed. It enables us to detect the lost moments caused by the aerodynamic trail of the teeth in the lubricant inside the gearbox. In order to reduce computation times, a sector corresponding to two teeth is considered (figure 3) and modelled by Gambit. Periodicity condition allows us to find the total pressure and viscous moments on the gear periphery. The coordinates of the teeth are recovered by a suitable program (Fluent, 2006). The points defining the teeth geometry are then inserted in Gambit.

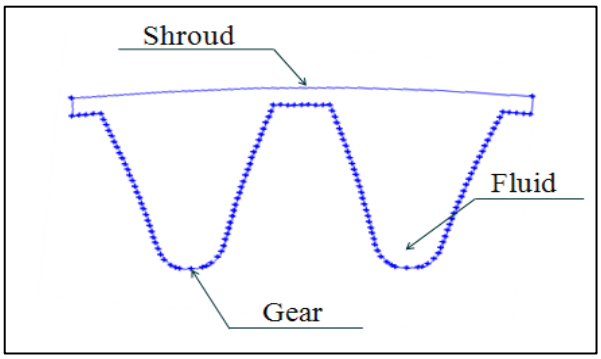

Fig.3 Design model with Gambit

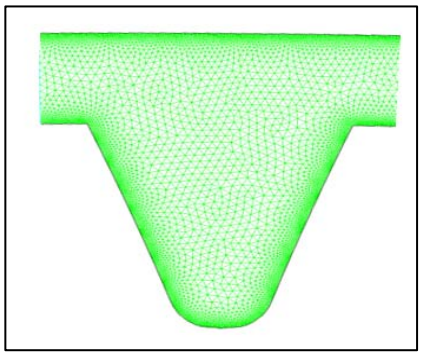

Fig.4 Mesh

An unstructured triangular mesh is adopted (figure 4). A size function is used to create a refinement around the gear teeth and peripheral shroud. This choice of meshing allows the minimization of the total number of element in order to have a reasonable computing time. The number of cells is 20942.

2.2.2 Boundary conditions and discretization scheme

Table 2, 3 and figure 5 present the boundary conditions considered for the simulations.

Peripheral shroud	Stationary wall
Gear teeth	Rotating wall
Limits of the gear	Periodic
Free space	Fluid

Table2. Boundary condition in the pre-processor Gambit

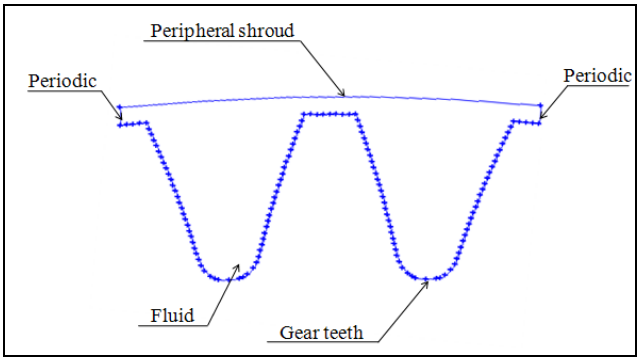

Fig.5 Boundary conditions of the model

Solver	Implicit
Space	2D
Time	Steady
Velocity formulation	Absolute
Viscous model	RSM (Reynolds stress model)
Options	Enhanced wall treatment

Table3. Boundary conditions in Fluent

Table 4 present the adopted discretization schema:

Pressure velocity coupling	SIMPLE
Pressure	Presto
Momentum	Second order upwind
Turbulent Kinetic Energy	Second order upwind
Turbulent Dissipation Rate	Second order upwind
Reynolds Stresses	Second order upwind

Table4. discretization parameters

2.3 Computation of the windage power loss

The total WPL can be computed using the following formula:

For peripheral WPL (Diab et al.,2004):

$$P_{perip} = \frac{1}{2} C_m \rho \omega^3 R^5 \qquad (11)$$

where ρ is the fluid density [kg /m3], ω the rotational speed [rd/s] and R=D/2 the gear outer radius (m).

The adimensioned torque moment Cm can be expressed by (Seetharaman, 2009):

$$C_m = \frac{Tm}{0.5\pi\rho\omega^2 r_i^4 h} \qquad (12)$$

with Tm [Nm] is the torque given by Fluent, ri: the gear inner radius [m] and h the thickness of gear edge [m].

For WPL on gear sides (Seetharaman, 2009):

$$P_{sides} = 15000\left(\frac{N}{1000}\right)^3\left(\frac{D}{2.54}\right)^5 \qquad (13)$$

where N is the shaft speed [rpm].

The total WPL is then recovered by:

$$P = P_{perip} + P_{sides} \qquad (14)$$

3 Results and discussion

3.1 Influence of mesh density

In order to observe the influence of mesh on the quality and the convergence of the solution, we implemented three types of mesh densities were implemented: the first one with 4704 cells, the second with 12074 cells and the third with 13637 cells (Figure 6). The objective is to select the suitable type of mesh that offers both a good quality of solution with reasonable computation time.

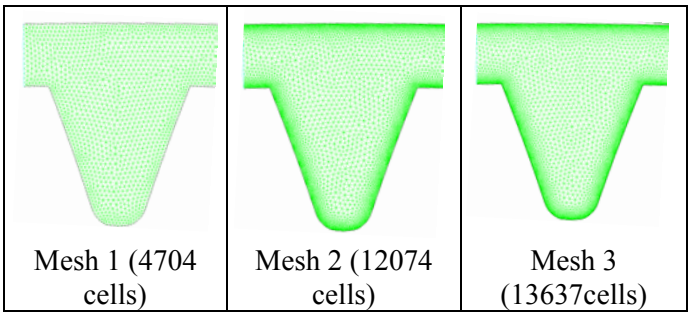

Fig.6 Representation of the three mesh densities

Considering gear no. 1 with distance of 1mm to the gearbox, the air as a fluid in the free space, and using the RSM turbulence model, the total windage power loss is computed with the three mesh types and represented in figure 7.

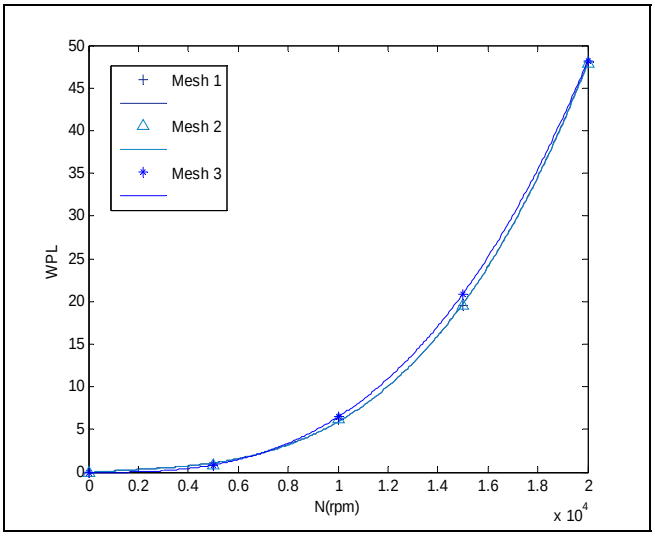

Fig.7 Total windage power loss for the three types of mesh

Figure 8 shows the static pressure cartographies for the three types of mesh density for a rotational speed of 20000 rpm.

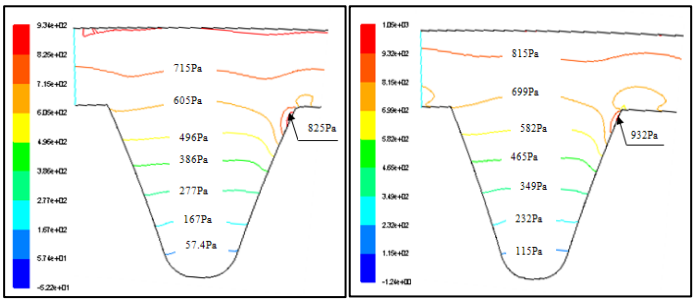

Mesh 1 (5876 cells) Mesh 2 (14552 cells)

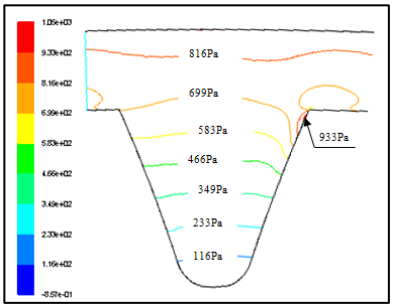

Mesh 3 (13637 cells)

Fig.8 Static pressure cartographies for the three types of mesh densities

It is noticed that the simulated static pressure profiles are almost identical which leads to an identical windage power loss induced by the effect of pressure and viscosity. The mesh density affects the computing time and the number of iterations needed for the convergence of the solution. For example, when the rotational speed is 20000 rpm:
-For mesh type 1 (Mesh1) the convergence is reached after 5925 iterations,
-For mesh type 2 (Mesh2) the convergence is reached after 10339 iterations,
-For mesh type 3 (Mesh3) the convergence is reached after 10742 iterations,

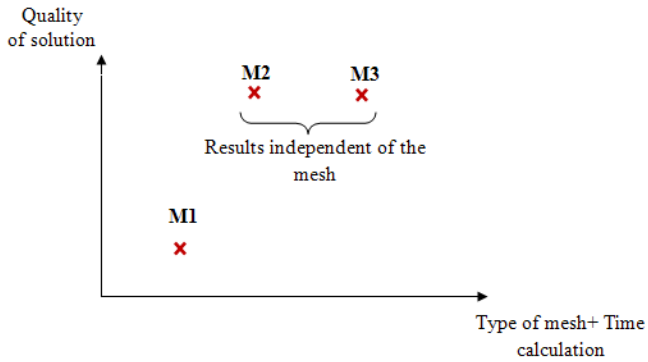

Fig.9 Evolution of the quality of the solution according to the type of mesh and computation time

We have noticed that from mesh type 2 the quality of the solution remain constant (figure 9). So for all the simulations, mesh type 2 will be used because it meets the required criteria. This type of mesh is characterized by a refinement near the gear teeth in order to reduce the loss of information in areas with a high pressure gradients and speeds.
In figure 8 (Mesh 2), the pressure gradients increase

from 115 Pa to 815 Pa when going from the root diameter to the outside diameter of the gear. This difference in pressure induces the creation of aerodynamic drag forces, i.e. the moments of drag due to the effect of pressure and viscosity. This resistive torque to the movement of the gear causes the windage power losses which tend to increase with the gear rotational speeds.

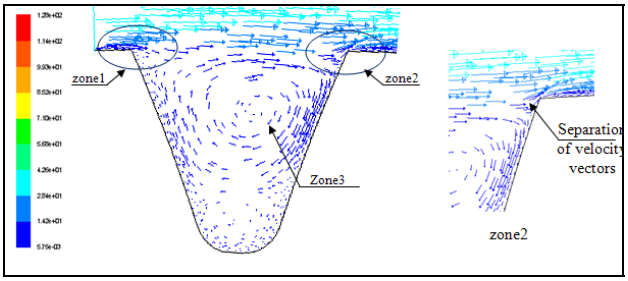

Fig.10 Relative velocity cartographies for the mesh type 2 with a rotational speed of 20000 rpm

Figure 10 shows the relative velocity cartographies for the mesh type 2 when the rotational speed is 20000 rpm. Three significant zones can be distinguished in the velocity profiles:
-Zone 1: in this tooth edge the velocity vectors remain tangent to the teeth outer diameter. The same direction is observed in the free space between teeth and gearbox.
-Zone 2: concerns the opposite edge in which a separation of the velocity vectors is observed. In this zone was also observed a high pressure gradient as show in figure 8
-Zone 3: situated in the inter teeth space. The velocity vectors present a vortex shape.

3.2 Influence of the number of the teeth

In order to observe the influence of the number of the teeth on the evolution of the windage power loss, we carried out two simulations. The first one with a gear n°1 (120 teeth) and the second one with gear n°4 (25 teeth). Figure 11 shows the total windage power loss for the two gears.
We noticed that the power losses for the gear n°4 are very weak for all the rotational speed compared with those of the gear n°1. This fact is explained by the increase of the active surfaces being opposed to the air flow and consequently amplification of the power loss.
For a rotational speed of 20000 rpm, the static pressure cartographies for the two types of gears are given in figure 12.

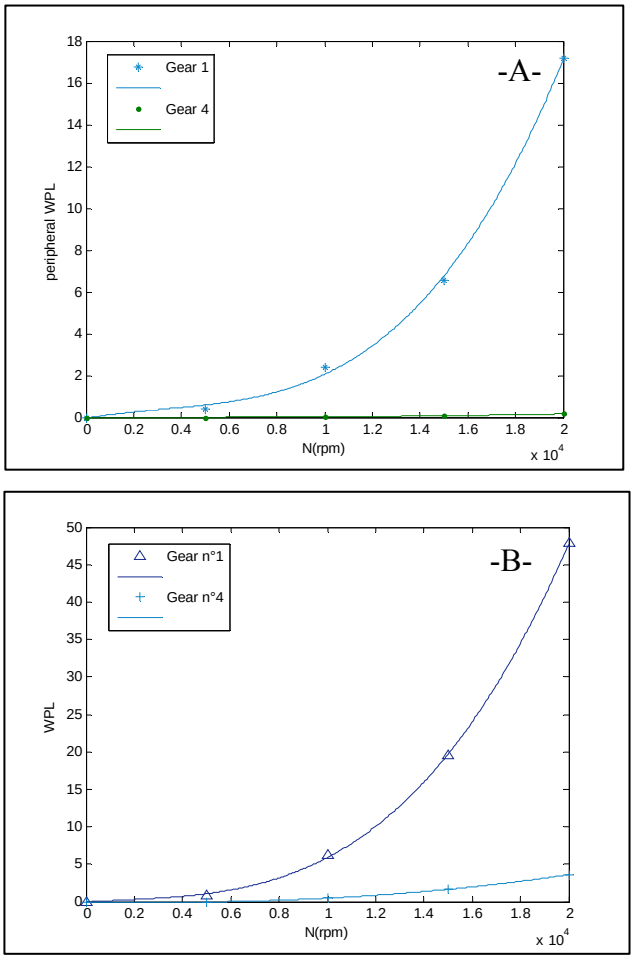

Fig.11 Peripheral (A) and total windage power loss (B) for the gear n°1 and n°4

Increasing the number of the teeth causes a significant change of the pressure starting from the root diameter of the gear to the outside diameter. This variation is as follows:
-For the gear n°1 (120 teeth): 115 Pa to 815 Pa,
-For the gear n°4 (25 teeth): 18.9 Pa to 174 Pa,
This increase induces a significant variation of pressure gradients at the tip of the tooth gear.

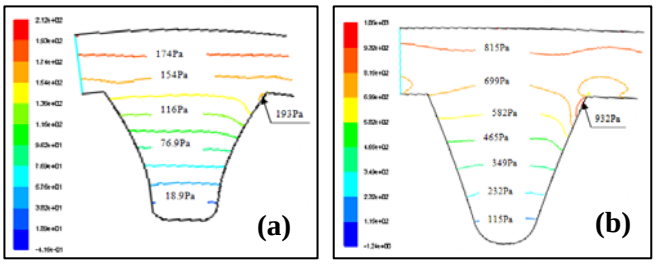

Fig.12 Comparison between the static pressure cartographies for two types of gear: Z=25 teeth (a) and Z=120 teeth (b)

3.3 Influence of the module change

To implement the influence of the gear module on static pressure cartographies and on the WPL, two simulations are performed with gear n°4 (m=1mm) and gear n°2 (m=8 mm).

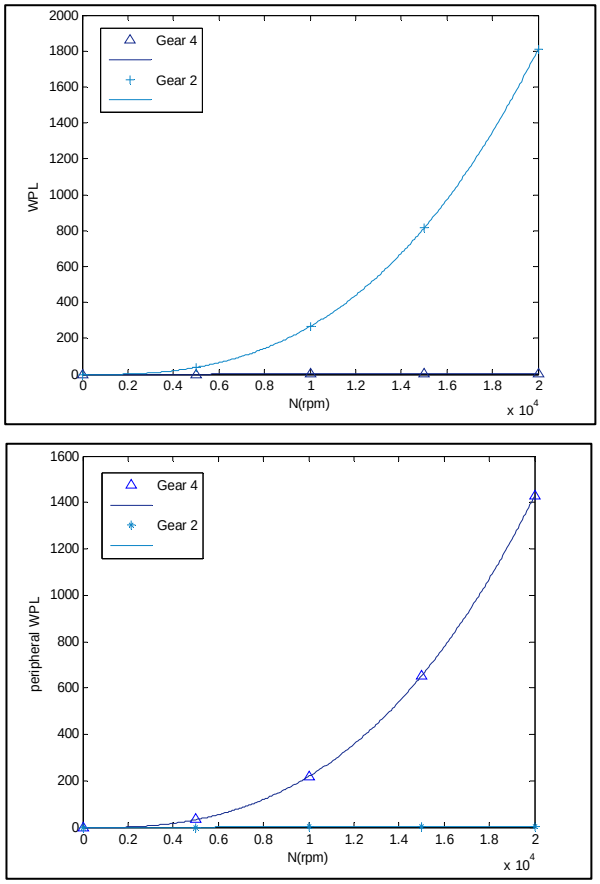

Fig.13 The total windage power losses for the gears n°4 and n°2

Changing the gear module from 2 mm to 8 mm results in a substantial increase of the total power loss (figure 13). This change is induced by the extension of the height of teeth (the distance between the root diameter of the gear and its outside diameter), that explains why the peripheral losses are rather enormous compared to those on the side losses.

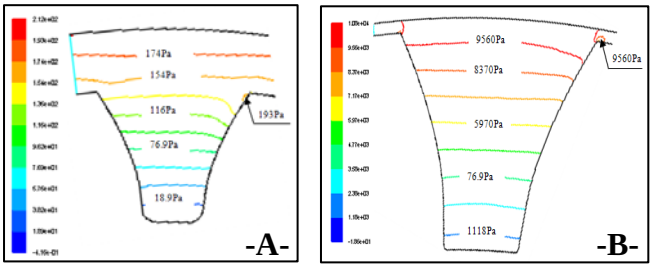

Fig.14 Comparison between the static pressure cartographies for two types of gear : m=1 mm(a) and m=8 mm(b)

Figure 14 shows the static pressure cartographies for the two module cases

The increase of the inter-teeth free space due to module increase induces a significant variation of the pressure. This variation passes:

-For the gear n°4: from 150 Pa to 629 Pa,

-For the gear n°2: from 1180 Pa to 9560 Pa,

3.4 Influence of the lubrication in the gearbox

In the gearbox of gear transmission, the fluid around the gear can be a mixture of air and vapor of oil made up of droplets of various sizes, its density will depend on the voluminal oil concentration in the air. An equivalent density of the oil-air mixture can be expressed as function of the density of each fluid. For a 3% ratio air-oil, the equivalent density and viscosity can be determined by (Neil et al., 1980):

$$\begin{cases} \rho_{equi} = \dfrac{(1)\rho + (34.25)\rho_{air}}{35.25} \\ \mu_{equi} = \dfrac{(1)\mu + (34.25)\mu_{air}}{35.25} \end{cases} \qquad (14)$$

Figure 15 shows an important increase of the power loss when air is changed to air-oil mixture for the gear n°1. As an example, for a rotating speed of 20000 rpm, the losses grow from 50 to 700W. This rise in the power loss is explained by the existence of a strong pressure gradient (figure 16) between the gear teeth which is about 15300 Pa for the air-oil mixture, while it does not exceed 699 Pa in the case of the gear rotating in the air.

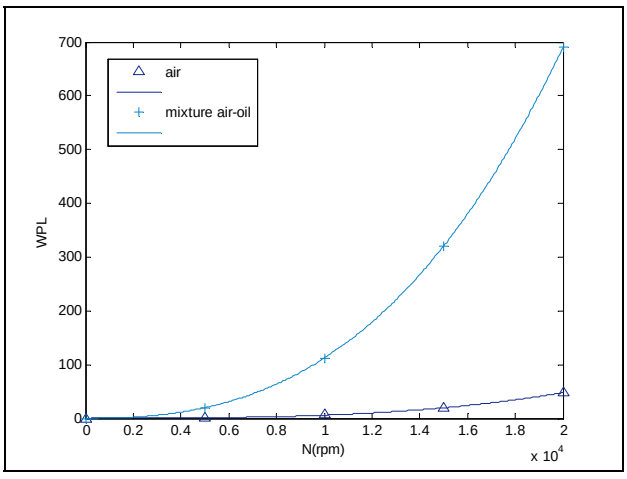

Fig.15 The windage power losses of the gear teeth

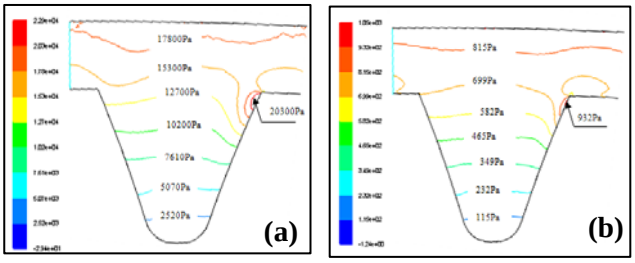

Fig.16 Comparison between the static pressure cartographies of simulation on the gear for two types of lubrication: (a) mixture air-oil and (b) air

3.5 Influence of the addendum modification on the gear teeth

In this section the influence of an addendum modification on the power losses is scrutinized. Figure 17 shows the change of the addendum factor from 0 to 0.5 when using gears n°2 and n°3.

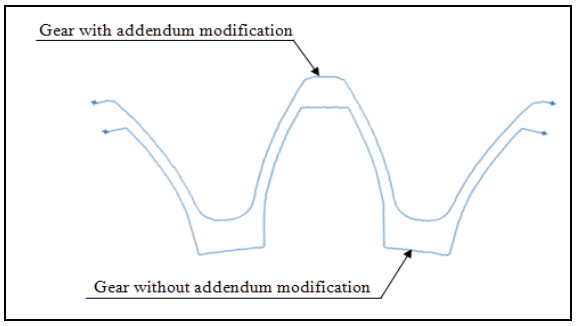

Fig.17 Comparison of the geometry of the gear teeth with and without addendum modification

The change of the addendum modification presents three principal interests (Fedala, 2007):
-The increase of the bending resistance by increasing the section of embedding,
-The optimization of the specific slips to decrease

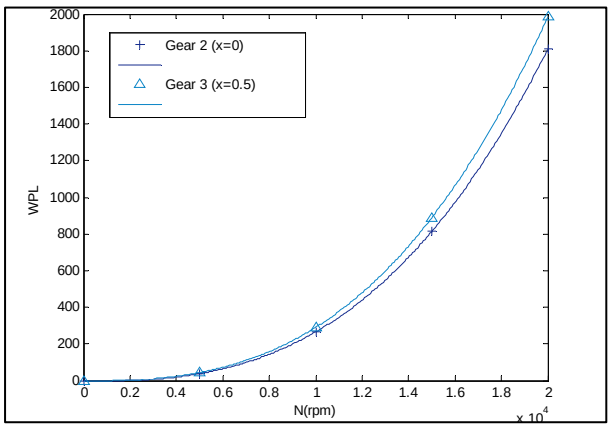

erosion on the small gear of the gears transmission
-Ensuring a fixed distance between centres,

Figure 18. Windage power losses of the gear teeth for both cases of addendum modification

The addendum modification of gear teeth induces a light increase in the total power loss at high speed. This increase is due primarily to a variation of the pressure gradients between the outside diameter of the teeth and the gear box when making an addendum modification of 0.5, as shown in figure 18. For a rotational speed of 20000 rpm, the static pressure cartographies for the two types of gears are given in figure 19. It noticed higher gradients of pressure around the teeth outer diameter.

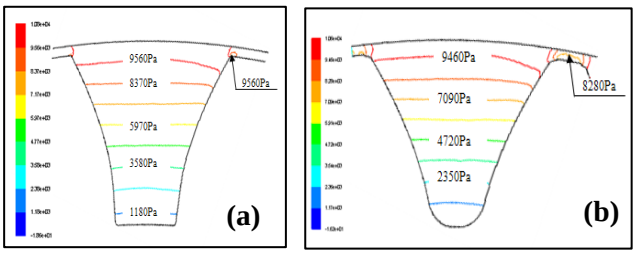

Figure 19. Comparison between of static pressure cartographies simulated on a gear for both cases of addendum modification: x=0 (a) and x=0.5(b) (2000rpm)

4 Conclusion

The windage power loss due to the effect of aerodynamic trail of the teeth in the air-lubricant mixture is a very complex phenomenon which involves several aspects (rotational speed, the shape of tooth, lubrication, the number of tooth, the module). In order to study the influence of each parameter on the amount of power loss, we proceeded to the resolution of the equilibrium equations of the assessment associated with the studied system. As the analytical solution is almost impossible especially in the turbulent case, where the equations are nonlinear, we adopted a numerical resolution. To this effect, the finite volume method was used with a two-dimensional model of a spur gear. The computations were carried out using the computation fluid dynamics code Fluent "6.3.26 ".
As results the viscous moment used to compute the windage power loss. It is also possible to plot the cartographies of pressure and velocity field. The main remarks can be summarized as flows:
-Increasing the rotational speed of the gear has a prevalent influence on the growth of moment and consequently on the power loss. This power lost induced a reduction in the efficiency of the gears.
-The presence of the teeth is the principal source of the increase of the pressure gradients especially on the inter-teeth space. This rise induces the increase of the effect of the aerodynamic trail which

amplifies the resistance of the surrounding fluid against the rotation of the gear.
-Gear lubrication type has an important influence on the windage power loss.
Future work will focus on a three dimensional model of the gear set. The objective will be the shape optimization of the gear body in order to minimize the windage power loss.

References:

[1] Al-Shibl K., Simmons K., Eastwick C. N. : Modeling Gear Windage Power Loss From an Enclosed Spur Gears, *Proc. Inst. Mech. Eng., Part A*. 221(3), 331–341 (2007).
[2] Chaari F., G. Kantchev, M. Haddar : Numerical computation of the mechanical efficiency of a spur gear system, *Eng. Comp. Mech*. 163, 83-90 (2010).
[3] Daly B.J., Harlow F. H.: Transport Equations in Turbulence, *Phys. Flu,* 13, 2634-2649 (1970).
[4] Dawson P.H. : Windage loss in larger high-speed gears. *Proc. Inst. Mech. Eng.,* 198A(1), 51-59 (1984).
[5] Dawson P.H: High-speed gear windage, *GEC Rev.* 4(3), 164-167 (1988).
[6] Diab Y., Ville F., Velex P: Windage losses in high speed gears», preliminary experimental and theoretical results, *ASME, J. Mec. Des.* 126, 903-908 (2004).
[7] Diab Y. : Analyse des Pertes de Puissance dans les Transmissions par Engrenages à Grande Vitesse, applications aux réducteurs industriels et aux machines textiles», *PhD, INSA de Lyon* (2005).
[8] Eastwick C.N., Johnson G.: Gear Windage *: A Review, ASME J. Mec. Des.,* 130 (2008).
[9] Fedala D., Simulation numérique des écoulements internes dans les turbomachines. cao-dao des turbomachines*, Lecture, Arts et Métiers ParisTech* (2007).
[10] Fluent 6.3.26, *User's Guide, Fluent Inc.* (2006).
[11] Kantchev G., Baccar W., Chaari F., Haddar M.: Analytical computation of the mechanical efficiency of compound mechanical systems», *Mach. Dyn. Prob.,* 33(2), 55-75 (2009).
[12] Lien F.S., Leschziner M. A., Assessment of Turbulent Transport Models Including Non-Linear RNG Eddy-Viscosity Formulation and Second-Moment Closure*, Comp. Flu.,* 23(8), 983-1004 (1994).
[13] Neil E. A and Loewenthal S. H.: Spur-Gear-System Efficiency at Part and Full Load», *NASA Technical Paper 1622, Technical Report* 79-46 (1980).
[14] Seetharaman S.: An Investigation of Load-Independent Power Losses of Gear Systems, *PhD, Ohio State University* (2009).
[15] Townsend D. and Dudley: *Gear Handbook, Second Edition, McGraw-Hill Inc*. (1992).